Periodic Density Functional Theory Calculations for Na-doped Quasi-one-dimensional Polyacetylene Chains

ARTICLE *in* THE JOURNAL OF PHYSICAL CHEMISTRY C · APRIL 2008

Impact Factor: 4.77 · DOI: 10.1021/jp077426l

4 AUTHORS, INCLUDING:

Roberto Bernal
Metropolitan Autonomous University
19 PUBLICATIONS **110** CITATIONS

Periodic Density Functional Theory Calculations for Na-doped Quasi-one-dimensional Polyacetylene Chains

A. Ramírez-Solís* and B. Kirtman

Department of Chemistry and Biochemistry, University of California at Santa Barbara Santa Barbara, California, 93106-9510

R. Bernal-Jáquez and C. M. Zicovich-Wilson

Departamento de Física, Facultad de Ciencias, Universidad Autónoma del Estado de Morelos, Cuernavaca, Morelos, 62210 México

Received: September 14, 2007; Revised Manuscript Received: April 6, 2008

We report periodic B3LYP/6−31G** density functional theory calculations on Na-doped quasi-one-dimensional *trans*-polyacetylene (PA) chains at various dopant concentrations. The chains are modeled using $C_{2m}H_{2m}Na_2$ unit cells (m = 11, 13, 21, and 31). Our main purpose is to compare with previous calculations on Li-doping. Properties compared include geometries, atomic charges, dopant binding energies, band structures, densities of states, and nature of binding. In contrast with Li, the Na-doped chains are dissociative at concentrations of Na/C ≥ 1/9, and the bond length alternation is reduced for Na-doping as compared to Li-doping. The most significant differences are the binding energies and the appearance of a narrow isolated unoccupied band within the PA $\pi-\pi^*$ gap in the case of Na-doping. This intragap band is predominantly composed of Na(3s,3p) atomic orbitals.

I. Introduction

The properties of semiconducting π-conjugated polymers are strongly modified when they are doped with electron donors or acceptors. Not only is there a huge enhancement of the conductivity,[1–5] but a major increase in the (non)linear electric susceptibilities is also indicated by recent ab initio calculations.[6–12] It is of interest to establish structure/property relationships for these systems based on quantum chemical treatments. Indeed, the key role played by topological/geometrical charged solitons in their conductivity was first suggested by Su, Schrieffer, and Heeger (SSH)[13] who utilized a Hückel-like model for a doped (*trans*-) polyacetylene (PA) chain. According to their theory, these solitons are formed as a result of charge transfer to or from the chain. In first approximation, the dopant serves merely as the charge source or sink. Like the treatment presented here, SSH considered only an isolated one-dimensional (1D) chain, thereby omitting solid state effects. Although this precludes direct comparison with experiment, the 1D system is a useful starting point for an eventual full understanding of the three-dimensional (3D) solid.

There have been many theoretical studies of doped 1D PA chains, and other π-conjugated semiconductors, in the intervening years. However, only in the past few years have ab initio calculations been undertaken and only recently has the dopant been explicitly taken into account.[11,12,14] Using alkali atoms as the dopant, these treatments clearly establish a substantial dependence of the (non) linear electric susceptibilities upon the particular alkali. In the forerunner to this paper,[15] the first periodic band structure calculations were carried out as a function of dopant concentration for, in that instance, Li-doped PA chains. For Li-doping, Mulliken charges suggested significant covalent bonding (see later however) between the dopant and the carbon chain. In addition, the bonding was found to be a mixture of localized interactions at the dopant site and delocalized interactions with the PA π system. Importantly, the resulting band structure did not exhibit a midgap C(π) state associated with soliton formation.

TABLE 1: Comparison of C−C Distances for Li and Na-doped PA Chains (Å) and the Corresponding Bond Length Alternation (BLA) Values from the Optimized B3LYP/6-31G Periodic $C_{2m}H_{2m}M_2$ (m = 13; M = Li, Na) Structures[a]**

bond	Li (BLA)	Na (BLA)
C(0)−C(1)	1.409	1.408
C(1)−C(2)	1.43 (0.021)	1.422 (0.014)
C(2)−C(3)	1.369 (0.061)	1.378 (0.044)
C(3)−C(4)	1.429 (0.06)	1.422 (0.044)
C(4)−C(5)	1.368 (0.061)	1.374 (0.048)
C(5)−C(6)	1.429 (0.061)	1.423 (0.049)
C(6)−C(7)	1.368 (0.061)	1.374 (0.049)

[a] Only one-fourth of the chain distances are shown because all others are symmetry related. C(0) labels the central carbon trigonal doping site.

All of our conclusions in the previous study were based on closed shell, that is, spin-restricted, calculations. One might question whether the electronic structure contains significant biradical character that was overlooked. It turns out that such is not the case, as will be demonstrated in the following section.

It is of interest, then, to see how the closed-shell theoretical periodic band structure results are altered when Li is replaced by an alkali atom with a lower ionization potential. In that vein, we report here on Na-doping as a function of concentration. Because the computational methods are essentially the same as before, only a brief review is presented in Section II, along with a justification of the closed-shell treatment. Then, focusing on the comparison between Li and Na, we go on to describe the

* Corresponding author: alex@buzon.uaem.mx. On sabbatical leave from Universidad Autónoma del Estado de Morelos.

10.1021/jp077426l CCC: $40.75
Published on Web 05/31/2008

TABLE 2: Comparison of B3LYP/6–31G Geometries and Binding Energies for Li- and Na-doped PA Chains[a]**

	unit cell length		M−C distance		binding energy	
dilution *y*	Li	Na	Li	Na	Li	Na
1/11	27.20	27.35	2.064	2.391	31.96	14.68
1/13	31.98	32.30	2.066	2.419	33.49	15.82
1/21	51.96	51.96	2.067	2.420	36.74	17.41
1/31	76.72	76.92	2.067	2.441	38.03	18.16

[a] The Li−C and Na−C distances are to the nearest carbon. All lengths are in Ångströms and the binding energies are in kcal/mol per dopant atom.

TABLE 3: B3LYP Alkali Atom Charges for Li- and Na-doped PA Chains Obtained with Different Basis Sets and Schemes for $C_{11}H_{13}M$ (M = Li, Na) Clusters Using the Geometry of the Infinite Periodic Chain[a]

population	6−31G**			6−311+G**	
scheme/basis	Li	$NaC_{11}H_{13}$	$Na_3C_{33}H_{35}$	Li	Na
Mulliken	0.341	0.551	0.618	0.431	0.801
ChelpG	0.515	0.681	0.687	0.517	0.681
Merz−Kollman	0.618	0.729	0.733	0.632	0.734
NPA	0.927	0.949	0.947	0.934	0.966

[a] For the 6-31G** basis, the Na second column compares results obtained with the larger $Na_3C_{33}H_{35}$ cluster for the central Na atom.

results for geometry, atomic charges, and binding energies in Section III.A, whereas the band structure, density of states, and nature of binding are discussed in Section III.B. Finally, we close with a summary of our key conclusions and some perspectives on future work.

II. Review of Computational Procedures

In almost all respects, the computational methods employed are the same as in our previous paper on Li-doping.[15] Again, CRYSTAL2006[16] was used to obtain the B3LYP/6−31G** electronic structure of periodic chains built from a $M_2C_{2m}H_{2m}$ unit cell, where M = Na is the alkali atom, and the integer *m* determines the doping level, *y* = Na/C atom ratio. The geometry optimizations were done using the rod group $P2_1/m$, which implies a symmetric chain with inversion symmetry with equal intracell and intercell Na−Na distances. This choice is consistent with finite cluster optimizations on $Na_3C_{33}H_{35}$. (cf. Figure 6). We examined only uniformly doped structures, which requires that *m* must be odd, as previously discussed.[15] In particular, we chose the values *m* = 7, 9, 11, 13, 21, and 31 with the doping level *y* = 1/*m*. Since *m* = 21, 31 were not considered earlier, these calculations were done for M = Li as well.

To test the adequacy of the 6−31G** basis set, we carried out exploratory calculations on an $M_2C_{14}H_{14}$ molecular cluster (M = Li, Na) using both the 6−31G** and 6−311G** basis sets. On the other hand, within the periodic scheme, the optimized geometries, the BLA patterns, the binding energies, and the band structures were compared for the $Na_2C_{22}H_{22}$ case using the 6−31G** and 6−311G** basis sets; because no significant differences were found with respect to results obtained with the larger basis set, we used the 6−31G** basis sets throughout this work.

Optimized geometries were obtained in the same manner as for Li-doped PA chains except that all calculations were done with the new option in CRYSTAL, where analytical gradients are computed for both cell and atomic parameters, thereby allowing accurate full geometry optimizations. In addition, we adopted several recently implemented techniques that have been designed to improve the convergence of the optimization processes in critical cases. These are the use of redundant internal coordinates that cancel the coupling between atomic and cell parameters, a starting semiempirical model Hessian, and the BFGS updating of the Hessian along the optimization.[16] Despite the use of a safer optimization method, for M = Na a larger number of iterations were needed to achieve convergence compared to the M = Li case. The number of optimization steps, 110 to more than 300, varies significantly with the Na/C ratio, and it strongly depends on the initial guess for the starting geometry, mainly the Na−C distance and the local angles that define the trigonal doping site. For the highest-doped cases the initial guess geometries were built using the corresponding optimized Li-doped unit cell (with a scaled Na−C distance using the Na ionic radius), but even in these cases two factors lead to very long optimization process: (a) the extreme flatness of the potential energy surface and (b) its nonquadratic behavior around the minima, mainly caused by the strong coupling between the Na displacement along the *x*-*y* plane and the changes in the backbone internal parameters, such as C−C distances and C−C−C-C dihedrals, that determine the BLA and the curvature of the carbon chain.

Atomic charges were determined, as before, from a Mulliken population analysis. However, these results were supplemented here by charges on finite clusters (see discussion in Section III.A) obtained from a natural population analysis (NPA),[17] as well as the Merz−Kollman (MK)[18] and CHelpG[19] electrostatic potential methods implemented in Gaussian98.[20]

The convergence of our (spin-paired) Kohn−Sham SCF calculations was considerably more problematic than for Li-doped chains. This was particularly so for light doping (*y* = 1/21 and 1/31) where convergence of the energy to better than 10^{-6} Hartree for the initial guessed geometry, taken from the shorter chains, was attained only after 320 cycles. We stress that, for these problematic cases, the main factor for slow SCF convergence is the initial local geometry of the Na atom at the trigonal doping site; we note that energy convergence to 10^{-5} Hartree can actually be reached in only 40−50 Kohn−Sham cycles but, after that, very small oscillations start to appear and lead to the slow convergence of the process mentioned above. Therefore, after the first few optimization steps have been done (and the local doping-site geometry has been refined), the SCF convergence becomes as fast as that found for the Li-doped PA. In such cases, the Broyden scheme[21] was used with a weight ranging from 0.7 to 0.05 Hartree, and a previous-cycle Fock matrix mixing of up to 60%.

To gain some insight as to the effect of spin-pairing, several tests were carried out on symmetric *y* = 1/7 and *y* = 1/13 M = Li finite chains (terminated with H atoms) at the infinite periodic chain geometry. It turns out that a spin-polarized UB3LYP/6−31G** treatment reduces to the spin-paired structure. Several different initial approximations were attempted with the same result in each case. In addition, complete active space SCF with 4 electrons in 4 orbitals (CASSCF(4,4)/6−31G**) calculations were carried out with the HOMO − 1, HOMO, LUMO, and

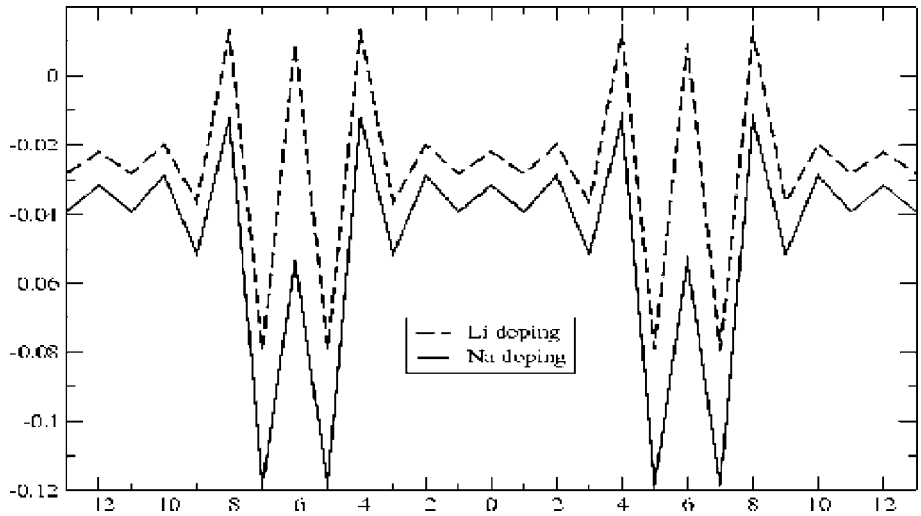

Figure 1. B3LYP/6−31G** Mulliken charges of CH units along uniformly doped periodic $C_{2m}H_{2m}M_2$ chains for $m = 13$ (M = Li, Na).

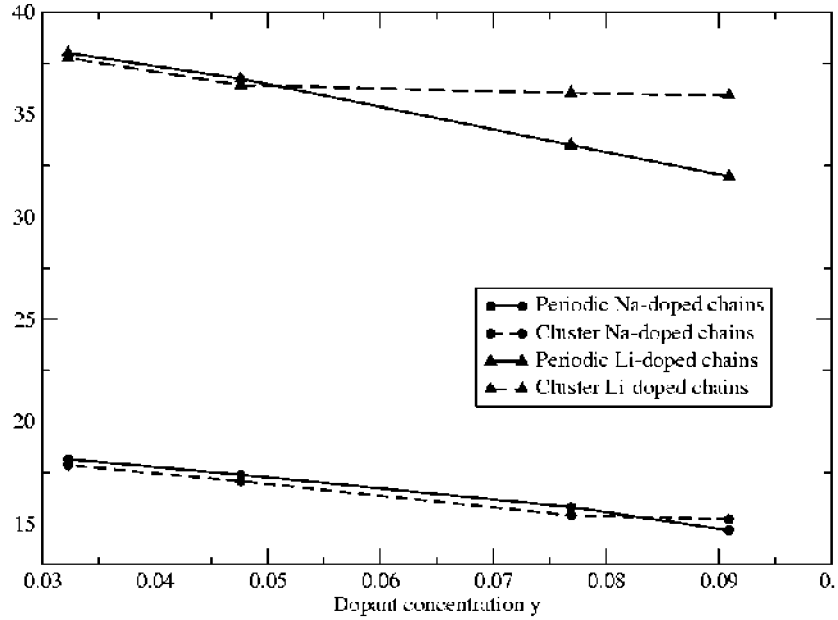

Figure 2. Metal binding energies per alkali atom (kcal/mol) as a function of doping concentration *y*. Full lines link periodic results, and dashed lines correspond to cluster calculations.

LUMO + 1 as active orbitals. This wave function allows the four electrons in the two Li-chain "bonds" to completely reorganize. Nonetheless, a single structure containing two doubly occupied orbitals was found to be strongly dominant (C0 > 0.966). Although these CASSCF orbitals are more localized than the two highest occupied (spin-paired) B3LYP/6−31G** orbitals, and the weight of the dominant structure is slightly reduced upon dilution, we conclude that the closed shell treatment is a reasonable approximation for the Na/C concentrations we study here.

III. Results and Discussion

A. Geometry, Atomic Charges, and Binding Energy (BE). At the doping levels $y = 1/7$ and 1/9, the periodic Na-doped chains are dissociative at the B3LYP/6−31G** level of treatment. To find if the local, semilocal, or nonlocal character of the exchange-correlation functionals plays a fundamental role in this respect, we have used the LDA (Slater + VWN5) and the GGA(BLYP) functionals and found the same result as with the B3LYP functional, that is, the dissociative behavior above $y = \text{Na/C} = 1/9$. This behavior may be compared with the finite chain RHF/6−31G results of Champagne et al.[12] where dissociation occurred for $y = 1/5$ but not for 1/7 or 1/9. Taking into account the different methodologies used in the two cases (finite vs. infinite periodic chains) we judge these calculations to be consistent with one another. From here on, only the doping levels $y = 1/11$, 1/13, 1/21, and 1/31 will be considered.

In all respects but two, the geometrical structure of the periodic doped chain is qualitatively and quantitatively similar for M = Na and M = Li. Thus, in both cases the carbon backbone varies sinusoidally in the direction perpendicular to the PA plane, and the metal binding site has a local trigonal structure with a reversal, in the sense of dimerization, on either side. Moreover, the corresponding C−C bond lengths along the chain (see Table 1 for $y = 1/13$) differ by less than 0.012 Å, whereas the unit cell lengths (see Table 2) lie within 1% of one another. However, the bond length alternation (BLA) is reduced for Na-doping as compared to Li-doping. Table 1 also includes a comparison for the $y = 1/13$ case, where the BLA reduction is from about 0.061 to 0.045 Å. This result remains about the

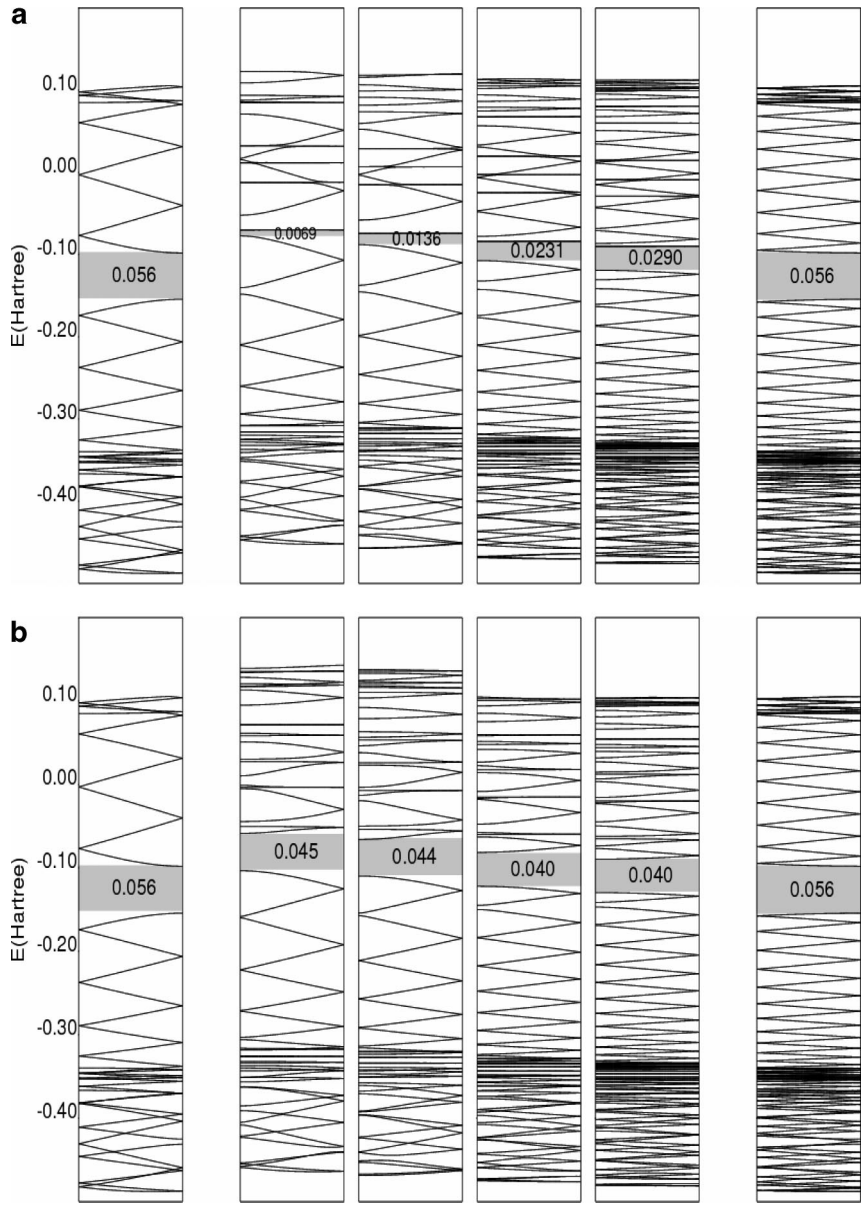

Figure 3. B3LYP/6−31G** band structures for uniformly doped $C_{2m}H_{2m}M_2$ chains (four middle panels, $m = 11, 13, 21, 31$) and undoped $C_{2m}H_{2m}$ panels on far left ($m = 11$) and far right ($m = 31$) periodic chains: (a) M = Na, (b) M = Li.

same regardless of the dopant level. The other significant difference is the metal−carbon distance, shown in Table 2. As expected, this distance is calculated to be longer (by 0.33−0.37 Å) for Na than for Li, which agrees well with the value obtained in ref 14 for a finite PA chain doped with a single metal atom.

For reasons discussed in our previous paper,[15] we note in passing that charge−strain relations cannot be meaningfully addressed by our computations.

Next, we examine the atomic charges. Although the Mulliken charge is not useful on an absolute basis, it has proved valuable in establishing trends. For positively charged solitons (no dopant counterions), it has recently been found[22] that most other population analysis methods, such as natural population analysis (NPA), yield similar values for the CH unit charges along the chain. On the other hand, the Mulliken and NPA charges on the metal atom in M−CH_3 and M−CCH turn out to be very different.[23] Hence, we decided to compare the several different methods mentioned in Section II for determining the alkali atom charge in Na- and Li-doped PA. To do so, it was necessary to use finite chain results. For validation purposes, an initial set of atomic charge calculations was carried out on $C_{11}H_{13}M$ clusters (C_s symmetry) using the geometry of the $y = 1/11$ periodic polymer, except for adding terminal H atoms.

Apart from the chain ends, the Mulliken charges obtained were very similar to those found for the periodic polymer. Thus, we proceeded with the finite chain comparison for the charge on the alkali atom shown in Table 3. As expected, the Mulliken values are quite sensitive to the choice of basis set, but the other schemes are not. Na transfers more charge to the chain than Li in all cases. However, in contrast with the other methods, NPA indicates nearly complete charge transfer and a consequent small difference between the Li and Na charges. On the basis of the significant difference in BLA between Li-doped and Na-doped chains, we are inclined to discount the NPA values. At this point, however, we cannot conclusively say that significantly greater charge transfer is associated with Na-doping. As an aside, we note that the calculated overall charge transfer for each method (Mulliken and NPA), as well as the charge distribution along the chain, is not significantly different when obtained from the CASSCF(4,4) wave function discussed in Section II.

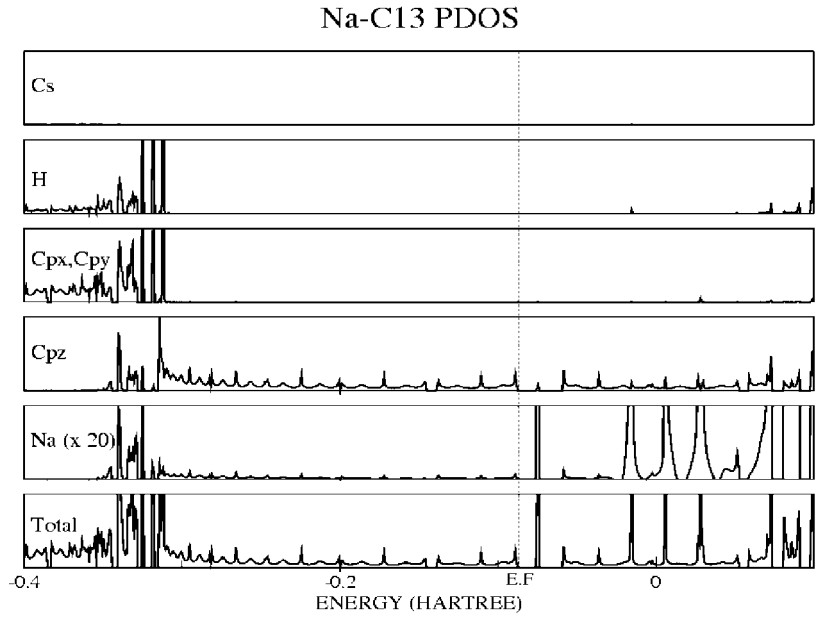

Figure 4. B3LYP/6−31G** total and partial DOS for Na-doping at the concentration $y = 1/13$. Na stands for Na(3sp) projection. Only valence bands are shown.

To test convergence of finite cluster charge transfer to the periodic value, we also studied Mulliken charge transfer on the $Na_3C_{33}H_{35}$ (corresponding to the 3/2 unit cell for $y = 1/11$) cluster using the same basis sets (see Table 3). We found that the Mulliken charge on the central Na (0.618) is almost exactly the same as the corresponding periodic value of 0.615 for the same Li/C ratio. We note that the charge obtained with the smallest possible cluster for $y = 1/11$ (involving a single Na and 11 carbon atoms) corresponding to 1/2 periodic unit cell model was 0.55; this clearly shows that the presence of two other Na atoms (one on each side placed 11 carbon atoms away and on the opposite side of the chain) does have a non-negligible effect on the overall charge transfer (around 10% more) at the central doping site. Therefore, long-range and delocalization along the chain seem to be important effects that cannot be properly reproduced by small single-doped molecular models.

As opposed to the overall charge transfer, the charge distribution pattern for the CH units along the chain is not very sensitive to the method of calculation or the size of the basis set. For that reason, the close resemblance between the distribution patterns obtained for Li- and Na-doping, illustrated for $y = 1/13$ in Figure 1, is regarded as meaningful.

The dopant binding energy (BE) was calculated as 1/2 the energy difference per unit cell between the bound system, on the one hand, and an isolated PA chain (with the same number of carbon atoms) plus two separated metal atoms on the other. The isolated chain and the bound system are each at their own optimized equilibrium geometry, and no correction was made for basis set superposition error. For Li at $y = 1/11$ and 1/13, the resulting values, given in Table 2, are slightly different from those previously reported.[15] This difference is due to the following improvements: (i) consistent use of the geometry optimization procedure wherein the cell length and the intracell atomic positions are fully coupled; (ii) imposition of additional symmetry to allow only uniform doping (rod group $P2_1/m$); and (iii) use of a very large number (60) of k-points in undoped PA calculations to ensure high accuracy. A plot of BE versus y for both alkali atoms (see solid lines in Figure 2) shows similar behavior (that is, parallel curves) in either case, with the extrapolated infinite dilution values being 38 kcal/mol for Li and 18 kcal/mol for Na. Thus, in general, the Li bond to the PA chain is about twice as strong as the Na bond. Increasing the dopant concentration lowers the BE. However, even at the highest concentration considered ($y = 1/11$), the effect of dopant−dopant interactions is relatively small, roughly 6 kcal/mol for Li and about half as much for Na. This is consistent with smaller through-bond contributions in the latter due to weaker bonding with the PA chain.

For comparison purposes we also carried out finite chain calculations on isolated unit cells extracted from the periodic polymer, as described above in connection with atomic charges. The results for the BE per alkali atom are also shown in Figure 2 (dashed lines). By inspection, one can see that the finite chain values closely agree with those of the infinite periodic chain in the limit $y \rightarrow 0$, as they should. In the case of Li-doping, the BE for periodic chains begins to deviate from that of the isolated unit cell at the concentration $y = 1/21$. This indicates that non-nearest neighbor intercellular effects are becoming significant. For Na-doping, that does not occur until $y = 1/11$.

In our previous paper,[15] the soliton formation energy (SFE) was calculated as the energy required to convert the equilibrium geometry for the neutral PA chain to the distorted chain geometry in the bound system. Because the distorted geometries for Li- and Na-doping are so similar, we did not repeat the SFE calculation here. Using the previous results we find that the sum of the binding energy and the SFE, which represents the energy released when the dopant bonds to the distorted chain, is around 24 kcal/mol for Na-doping. This is a small value compared to most bond formation energies. The SFE was computed without spin polarization; if it were included, the SFE (and energy release) would be even smaller.

B. Band Structure, Density of States, and Nature of Binding. B3LYP/6−31G** band structures for the undoped and uniformly doped chains are presented in Figures 3a for Na and 3b for Li. In the middle four panels, the dopant concentration decreases from $y = 1/11$ on the left to $y = 1/31$ on the right. Band structures of undoped PA are included for $m = 11$ at the far left and for $m = 31$ at the far right in order to allow the reader to visually compensate for the folding connected to the change in size of the unit cell.

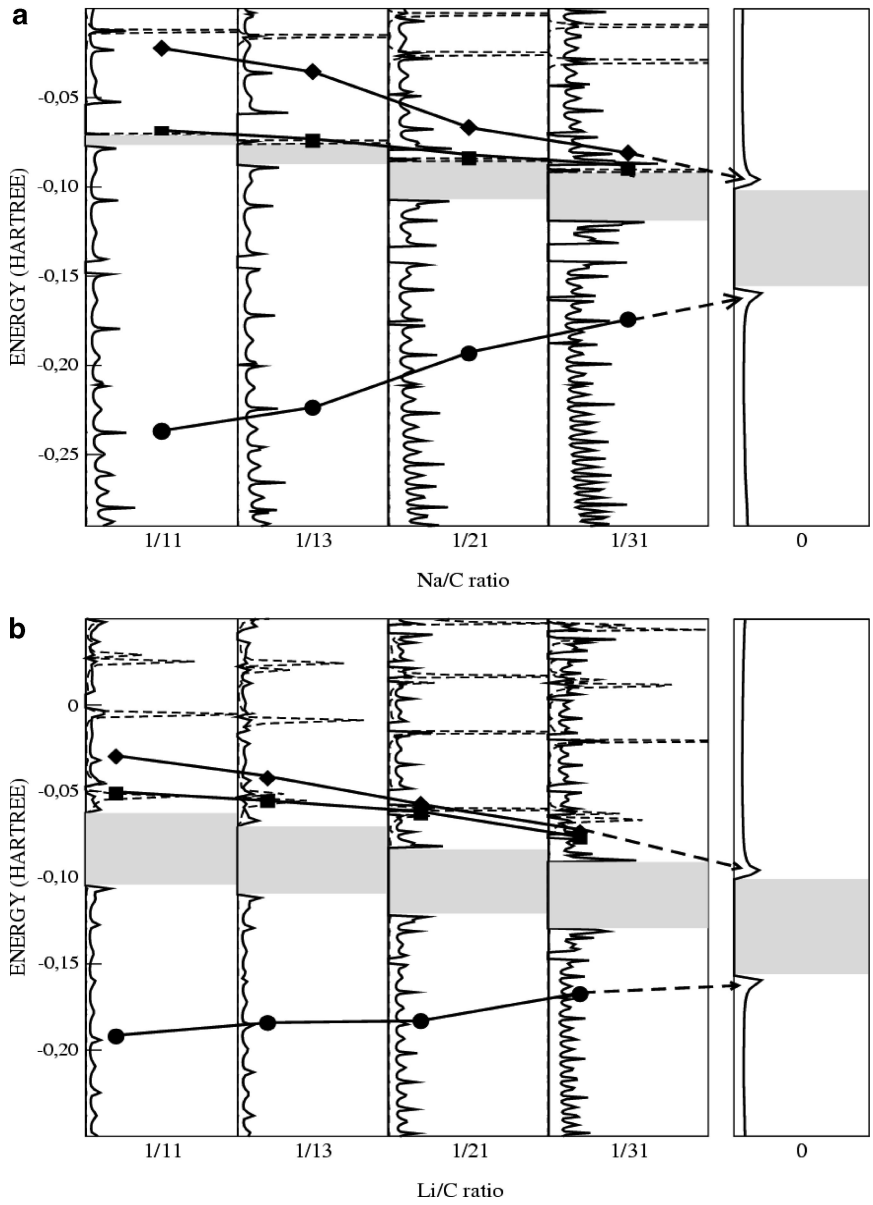

Figure 5. Evolution of selected bands/sub-bands in the vicinity of the PA band gap as a function of dopant concentration. The density of states is given along the vertical axis with contributions from alkali atom orbitals indicated by dashed lines. A C(π) sub-band (circles) that blends into the topmost valence band of undoped PA and a C(π*) sub-band that blends into the lowest conduction band (diamonds) of undoped PA are shown in each panel, along with the lowest unoccupied alkali atom band (squares). In each case the points are connected for visualization purposes only; (a) Na doping, (b) Li doping.

In many respects, the Li- and Na-doped chains have a similar band structure. There are some important differences, however, in the bandgap region. Of special interest is the narrow band that appears within the PA bandgap for Na-doping, but not for Li-doping, in Figure 3. It is noteworthy that this is not a $Cp_z =$ C(π) band (cf. ref 13). It is unoccupied and composed primarily of alkali atom orbitals. These two points are evident from Figure 4, which displays the total density of states (DOS) and several of its projections (PDOS) calculated for Na-doping at $y = 1/13$ by the scheme described in ref 24 (which is based on a Mulliken partitioning). The energy range in this figure includes the valence region as well as the lower conduction bands. In the intragap region the contribution of the C(π) orbitals is a small fraction of the total DOS, which primarily comes from Na atomic orbitals.

With increasing concentration, the intragap band moves from just below the bottom of the π* conduction bands to just above the π valence bands. This evolution is shown in Figure 5a along with the evolution of a sub-band that blends into the topmost π valence band of PA and another sub-band that blends into the lowest π* conduction band of PA. The key difference from Li-doping is that, for Li, the counterpart of the Na-doping intragap band remains within the π* conducting region, even at the highest dopant level.

Plots of the isodensity surfaces (at 0.1 e/Å^3; density normalized to total number of electrons in each unit cell) for these two bands, the Na-doping intragap band, and its Li-doping counterpart are given in Figure 6. These isosurfaces were computed by means of the XCrysDen[25] program coupled to the PROPERTIES code of the CRYSTAL suite of programs, which carries out an integration of the band density over the first Brillouin zone.

For Li-doping we see that there is substantially greater mixing with C(π) orbitals, which is consistent with larger covalent bonding character. On the other hand, as expected, the analogous

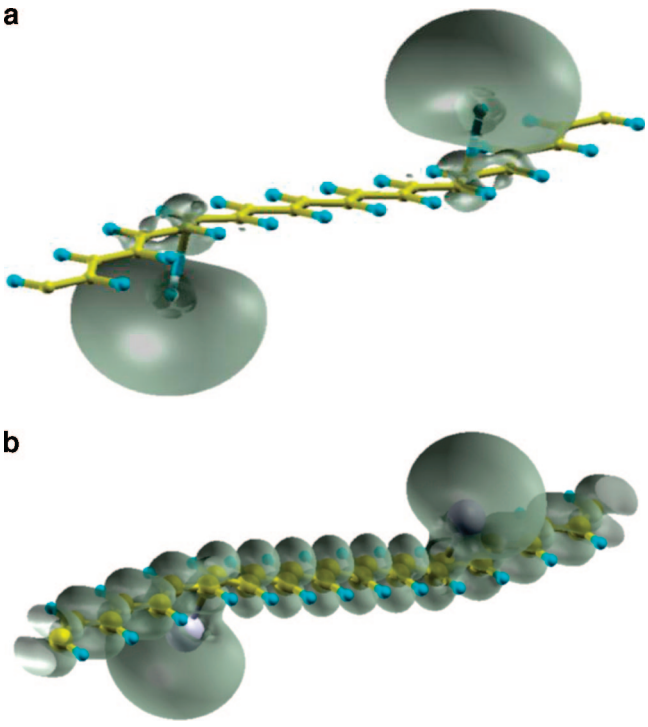

Figure 6. Isodensity surfaces at 0.1 e/Å^3 of the Na-doping intragap band and its Li-doping counterpart for $y = 1/13$. (a) Na-doping, (b) Li-doping.

plots for the highest occupied valence bands are virtually identical (not shown).

We turn, finally, to the nature of the binding between Na and the PA chain using the dopant level $y = 1/13$ as the basis for our discussion. The Na(3sp) PDOS given in Figure 4 shows a concentration of density in the energy region close to −0.33 eV. Of the total DOS in valence states, 45% lies in the narrow region from −0.34 to −0.31 eV and 47% lies in the region between −0.30 eV and the top of the valence band. Near −0.33 eV, the Na(3sp) PDOS largely tracks the C(π) PDOS, rather than the PDOS for Cp_x,Cp_y = C(p_σ) and H, which largely track one another. Hence, the localized bonding in this region is primarily Na−C(π) and H−C($p\sigma$). The π-bonding between Na and the PA chain has an almost equal mixture of localized and delocalized character. This is similar to what was found for Li-doping,[15] although the localized character is a bit less in the latter case (it should also be noted that for Li-doping the analysis was carried out at $y = 1/7$ rather than at $y = 1/13$). We also note here that the B3LYP calculation may overemphasize the degree of delocalization (cf. CASSCF results summarized in Section II).

IV. Conclusions and Perspectives

We have carried out periodic B3LYP/6−31G** calculations for 1D PA chains uniformly doped with Na atoms at varying concentrations, our main focus being a comparison with the corresponding Li-doped chains. In contrast with Li, the Na-doped chains are dissociative at concentrations of $y \geq 1/9$. For Na-doping the M−C distance is longer, with the difference being about 0.35 Å, and the BLA is reduced from about 0.060 to 0.045 A. With the exception of NPA, the charge analysis methods employed indicate that significantly more electronic charge is transferred to the PA chain as a result of Na-doping than Li-doping, although in either case the amount is considerably less than one electron per alkali atom. These charge transfer results are not definitive, but they are consistent with the significant difference found for the BLA.

In the limit of infinite dilution, the BE per Na atom is less than half of what it is for Li (18 vs 38 kcal/mol). Even at the highest concentration ($y = 1/11$) dopant−dopant interactions have a relatively small effect on the BE, which is lowered by about 6 kcal/mol for Li and by roughly half of that amount for Na-doping. The concentration-dependence for both alkalis is consistent with through-bond interactions. At a dopant level of $y = 1/11$, non-nearest-neighbor interactions start to become significant for Na, whereas for Li the onset occurs at about half of that concentration.

There are some key differences between Na- and Li-doping when it comes to the band structure. The most important, perhaps, is the intragap band found for the former but not for the latter. This band is unoccupied and is overwhelmingly composed of Na(3sp) orbitals; this result has also been found at the HF level for the $Na_2C_{26}H_{26}$ case. The corresponding band for Li-doping lies above the lowest PA conduction band. On the other hand, the binding to the PA chain is similar in character, although, of course, it is much weaker for Na. In either case the B3LYP results show roughly an equal mixture of localized binding at the dopant site and delocalized binding with the PA π system (the localized component is a bit smaller for Li).

Many different aspects of the electronic structure of doped PA, and other π-conjugated polymers, need further exploration. As far as individual PA chains are concerned, the effect of stronger donors is of interest, although we do not intend to pursue that aspect. More important, perhaps, would be the consideration of electron acceptors. This is not to mention the extension to (i) polymers with aromatic rings that will support polarons and bipolarons and (ii) dopants that are more spatially extended than alkali atoms.

A major goal is to study the electronic structure properties of more realistic 3D alkali-doped PA systems, and a reliable methodology for doing so is currently being developed. Further down the line it will be of interest to consider the dynamical behavior of the dopant atoms in these 3D systems. Given the large difference in binding energies (and, hence, mobility) in 1D, we may anticipate that, in 3D, the dynamical behavior of Li and Na may be quite different.

Acknowledgment. A.R.S. and C.Z.W. thank FOMES2000-SEP for unlimited CPU time on the IBM-p690 supercomputer at UAEM. A.R.S. and C.Z.W. also thank CONACYT (México) for support through project Nos. 45986 and 46983, respectively. R.B.J. acknowledges a postdoctoral fellowship through CONACYT project No. 45986. A.R.S. acknowledges support from the UCMEXUS/CONACYT program for a sabbatical year at UC Santa Barbara.

References and Notes

(1) (a) Shirakawa, H.; Louis, E. J.; MacDiarmid, A. G.; Chiang, C. K.; Heeger, A. J. *J. Chem. Soc. Chem. Commun.* **1977**, 578. (b) Chiang, C. K.; Fincher Jr, C. R.; Park, Y. W.; Heeger, A. J.; Shirakawa, H.; C Gau, S.; MacDiarmid, A. G. *Phys. Rev. Lett.* **1977**, *39*, 1098. (c) Chiang, C. K.; Gau, S. C.; Fincher Jr, C. R.; Park, Y. W.; MacDiarmid, A. G.; Heeger, A. J. *Appl. Phys. Lett.* **1978**, *33*, 18.

(2) Tsukamoto, J.; Takahashi, A.; Kawasaki, K. *Jap. J. Appl. Phys.* **1990**, *29*, 125.

(3) Cao, Y.; Smith, P.; Heeger, A. J. *Polymer* **1991**, *32*, 1210.

(4) Schimmel, T.; Reiss, W.; Gmeiner, J.; Schworer, M.; Naarmann, H.; Theophilou, N. *Solid Stat Commun.* **1988**, *65*, 1311.

(5) *Handbook of Conducting Polymers*, Skotheim, T. A., Ed.; Dekker: New York, 1986; Vols *I and II*.

(6) Olivera, L. N.; Amaral, O. A. V.; Castro, M. A.; Fonseca, T. L. *Chem. Phys.* **2003**, *289*, 221.

(7) Nakano, M.; Yamada, S.; Takahata, M.; Yamaguchi, K. *J. Phys. Chem. A* **2003**, *107*, 4157.

(8) An, Z.; Wong, K. Y. *J. Chem. Phys.* **2001**, *114*, 1010.

(9) An, Z.; Wong, K. Y. *J. Chem. Phys.* **2003**, *119*, 1204.

(10) de Melo, C. P.; Fonseca, T. L. *Chem. Phys. Lett.* **1996**, *261*, 28.

(11) Champagne, B.; Spassova, M.; Jadin, J. B.; Kirtman, B. *J. Chem. Phys.* **2002**, *116*, 3935.

(12) Spassova, M.; Champagne, B.; Kirtman, B. *Chem. Phys. Lett.* **2005**, *412*, 217.

(13) (a) Su, W. P.; Schrieffer, J. R.; Heeger, A. J. *Phys. Rev. Lett.* **1979**, *42*, 1698. (b) *Phys. Rev. B* **1980**, *22*, 2099.

(14) Champagne, B.; Spassova, M. *Phys. Chem. Chem. Phys.* **2004**, *6*, 3167.

(15) Ramírez-Solís, A.; Zicovich-Wilson, C. M.; Kirtman, B. *J. Chem. Phys.* **2006**, *124*, 244703.

(16) Dovesi, R.; Saunders, V. R.; Roetti, C.; Orlando, R.; Zicovich-Wilson, C. M.; Pascale, F.; Civalleri, B.; Doll, K.; Harrison, N. M.; Bush, I. J.; Arco, P. D.; Llunell, M. *CRYSTAL06 User's Manual*; Università di Torino: Italy, 2006; http://www.crystal.unito.it.

(17) Reed, A. E.; Weinstock, R. B.; Weinhold, F. *J. Chem. Phys.* **1985**, *83*, 735.

(18) Besler, B. H.; Merz, K.; Kollman, P. A. *J. Comput. Chem.* **1990**, *11*, 431.

(19) Breneman, C. M.; Wiberg, K. B. *J. Comput. Chem.* **1990**, *11*, 361.

(20) Frisch, M. J.; Trucks, G. W.; Schlegel, H. B.; Scuseria, G. E.; Robb, M. A.; Cheeseman, J. R.; Zakrzewski, V. G.; Montgomery, J., J. A.; Stratmann, R. E.; Burant, J. C.; Dapprich, S.; Millam, J. M.; Daniels, A. D.; Kudin, K. N.; Strain, M. C.; Farkas, O.; Tomasi, J.; Barone, V.; Cossi, M.; Cammi, R.; Mennucci, B.; Pomelli, C.; Adamo, C.; Clifford, S.; Ochterski, J.; Petersson, G. A.; Ayala, P. Y.; Cui, Q.; Morokuma, K.; Rega, N.; Salvador, P.; Dannenberg, J. J.; Malick, D. K.; Rabuck, A. D.; Raghavachari, K.; Foresman, J. B.; Cioslowski, J.; Ortiz, J. V.; Baboul, A. G.; Stefanov, B. B.; Liu, G.; Liashenko, A.; Piskorz, P.; Komaromi, I.; Gomperts, R.; Martin, R. L.; Fox, D. J.; Keith, T.; Al-Laham, M. A.; Peng, C. Y.; Nanayakkara, A.; Challacombe, M.; Gill, P. M. W.; Johnson, B.; Chen, W.; Wong, M. W.; Andrés, J. L.; González, C.; Head-Gordon, M.; Replogle, E. S. and Pople, J. A., *Gaussian 98 A.11.3*; Gaussian, Inc.: Pittsburg, PA 2002.

(21) (a) Broyden, C. G. *Math. Comput.* **1965**, *19*, 577. (b) Johnson, D. D. *Phys. Rev. B* **1988**, *38*, 12807.

(22) Monev, V.; Spassova, M.; Champagne, B. *Int. J. Quantum Chem.* **2005**, *104*, 354.

(23) Scalmani, G.; Bredàs, J. L.; Barone, V. *J. Chem. Phys.* **2000**, *112*, 1178.

(24) Pisani, C. Dovesi, R., and Roetti, C., *Hartree-Fock Ab Initio Treatment of Crystalline Solids,* Lecture Notes in Chemistry; Springer-Verlag: Berlin, 1988; Vol *48*.

(25) (a) Kokalj, A. *J. Mol. Graphics Modell.* **1999**, *17*, 176. (b) XCrysDen code is available at http://www.xcrysden.org.

JP077426L